Retinex-based And Phase Stretch Transformation For Robot Power Equipment Infrared Heat Map Enhancement And Segmentation

Xiaojing Hu[1*], Yanyong Han[1], and Rui Yang[1]

[1] School of Mechanical Engineering, Zhengzhou University of Science and Technology, Zhengzhou, 450015 China
[*] Corresponding author. E-mail: snowycry@qq.com

Received: Mar. 07, 2022; Accepted: Apr.17, 2022

In the maintenance of outdoor power equipment, the enhancement and segmentation of infrared heat map is the key to the intelligent development of diagnosis and troubleshooting in the future. This paper presents a new model for enhancement and segmentation of infrared heat map of power equipment in complex environment. Retinex image enhancement model is improved by region joint prior information constraint and gamma transform. In this paper, multi-scale structure reserved smoothing filter is proposed, and the filter size is constrained by phase stretch transformation. The new model can not only estimate and compensate the hidden noise, increase the contrast of the infrared heat map, but also eliminate the filtering edge dispersion phenomenon, which is suitable for power equipment segmentation of various sizes. Experimental results show that compared with other algorithms, the new model can obtain more complete and high contrast infrared heat map in complex environment, and has the performance of removing most background interference.

Keywords: Retinex, Phase stretch transformation, image enhancement, multi-scale structure reserved smoothing filter

http://dx.doi.org/10.6180/jase.202302_26(2).0009

1. Introduction

During the process of troubleshooting electrical equipment, conducting infrared diagnosis makes use of thermal infrared image is an effective method [1, 2]. By detecting target radiation, thermal infrared image obtains D-temperature distribution, i.e., thermography. In the infrared fault detection of outdoor power facilities, infrared images have the feature of low contrast and high background interference. Because of these features, it is necessary for convenient fault diagnosis to improve the sharpness and contrast of images, when detecting the fault of equipment according to the infrared images, and further isolating the target device [3, 4].

Processing based on spatial domain and transform domain are the primary existing methods of infrared heat map enhancement. The processing methods of spatial domain include histogram equalization and direct pixel transformation, etc., and the processing method of transform domain is mainly Fourier transform. The merits of these methods are simple and easy to operate, and the grand challenge is poor applicability and some areas lacking detail enhancement due to globality. Infrared image enhancement technique based on histogram bidirectional equalization and NSCT transform enhance high frequency part and low frequency part of the image differently, and has achieved a good effect in enhancing the sharpness of the image.

In recent years, Retinex algorithm [5] has good result in fog removal and image enhancement. However, Retinex algorithm regarded the illumination intensity as global uniformity, and obvious halo effect could be obtained in the region with large brightness difference. In recent years, single-scale Retinex and multi-scale Retinex algorithm [6] have improved this defect by taking points from any path in the image and adopting multiple iteration strategy to fit the light intensity of each region smoothly in segments. However, noise will increase in the process of enhancement,

resulting in color distortion in local regions.

Thermal faults of devices in the power system can be detected by determining whether the temperature of device components is abnormal. Due to different power equipment temperature has certain differences, there are a lot of equipment in the infrared heat disturbance, a convenient and effective method is to use gray-level threshold segmentation, such as use Otsu threshold gray [7, 8] of image segmentation, but for the temperature of different size, different equipment, it may cause local segmentation is incomplete.

In order to solve the problem of over-segmentation of images, Zou and Huang [9] proposed an infrared image segmentation algorithm based on fast-match algorithm, using template matching to approximate affine the target region, but this method can only identify a single object, and it is difficult to Match multi-size targets in complex scenes. Wang et al. [10] used k-means algorithm based on weighted Chebyshev distance for segmentation, but could only segment the part with lower gray level.

Based on the complicated operating environment, multi-disturber and small grayscale difference characteristics of power equipment under real environment. Our main contributions are as follows. In this paper, an infrared heat map enhancement and segmentation method suitable for power equipment in complex environment is proposed. Through changing local deviation to division of heat maps, the Retinex enhanced model is improved by using the joint prior information and gamma transform method to estimate and compensate image noise and improve the contrast of infrared heat map.

Then, the multi-scale structure reserved smoothing filter is proposed, and the Gaussian regular term is used to constrain the filter size, which can effectively eliminate the edge dispersion phenomenon with different sizes of equipment filter. The results verify that this method can maintain good segmentation integrity for multi-size devices in complex environment and remove most of the homogeneous background interference.

This paper is organized as follows. Section 2 displays the improved Retinex image enhancement model. Section 3 and section 4 detailed introduce the multi-scale structure reserved smoothing filter and phase stretch transformation. Experiments and analysis are shown in section 5 and the paper is concluded in section 6.

2. Improved retinex image enhancement model

Retinex theorizes that color is perceived by the human eye through the interaction of light and matter. Any image can be decomposed into illuminance component I and reflection component R. Illuminance component mainly reflects image illumination information, including color dynamic range. The reflection component represents the details of the image, including structural edge and texture information.

In this paper, the improved Retinex model determines the region type and performs the corresponding noise estimation and compensation for the reflection components by solving the local variation bias. The reflection component and incident component are solved by iterative reweighting method and gamma transform is performed on illuminance component. The improved Retinex model not only can suppress image noise but also improve the dynamic range of image gray.

2.1. Regional differentiation based on local variation bias

In the statistical standard deviation are commonly used to quantify the intensity of the data distribution, and the amount of local variation deviation [11, 12] can distinguish the size of deviation difference between different data distributions. By solving the gradient similarity between adjacent pixels of the image, the local variation bias can be applied to the task of distinguishing characteristics of image.

Defining the local variation deviation of x and y directions $\Re_{x/y}$ as follows:

$$\Re_{x/y} = \left| \frac{\partial_{x/y} S_\Omega}{\frac{1}{\Omega}\sum_\Omega \partial_{x/y} S_\Omega + \varepsilon} \right| \tag{1}$$

Where ω is an image processing unit with r×r pixel size. In order to improve accuracy, the size of ω area is set as 3×3 in this paper. $\partial_{x/y} S_\Omega$ is the x-direction and y-direction derivative of image blocks S_ω in the ω region. ε is a small positive number to avoid a zero in the denominator. Assume that the total change of image gradient in ω region is ξ_Ω to represent the intensity of pixel change in ω region:

$$\xi_\Omega = \left| \partial_x S_\Omega + \partial_y S_\Omega \right| \tag{2}$$

Suppose that the mean change of image gradient in ω region is S_Ω , as shown in the following formula, to represent the mean change gradient in this region:

$$\varsigma_\Omega = \left| \frac{1}{\Omega} \sum_\Omega \left(\partial_x S_\Omega + \partial_y S_\Omega \right) + \varepsilon \right| \tag{3}$$

$D_{x/y}$ is the difference between the total change in gradient and the average change in gradient:

$$D_{x/y} = \xi_\Omega - \varsigma_\Omega = \left| \partial_{x/y} S_\Omega - \frac{1}{\Omega} \sum_\Omega \partial_{x/y} S_\Omega \right| \tag{4}$$

As the pixel value of the edge part of the image hops obviously, compared with the texture and smooth area, the edge part has the characteristics of large gradient change and more similar gradient direction. Using the variation relationship between local change deviation and regional gradient, we can carry out regional recognition of the image. For the smooth region, the gradient in the region is basically 0, hence, $D_{x/y} \approx 0, \Re_{x/y} \approx 0$. For the texture region, the gradient inside the region changes little and is basically constant, hence, $D_{x/y} > 0, \Re_{x/y} \approx 1$.

For the edge region, the pixel values within the region vary significantly and the gradient values differ greatly, hence, $D_{x/y} > 0, \Re_{x/y} \approx 1$. According to the above judgments, by solving the x and y gradients of the infrared heat map sub-unit of the arrester (Figure 1-a), and calculating $\Re_{x/y}$ and $D_{x/y}$, the edge part of the equipment structure can be distinguished as shown in Fig. 1-b.

2.2. Retinex components estimation using joint prior

The real image in Retinex is formed by combining illuminance and reflection components. Phenomenon can be known from practical observation that: Objects of different materials show different surface brightness even when they get the same amount of light.

However, the intensity of light on the same object is basically the same, so it can be approximated that the light in the same area is unchanged. Taking advantage of this feature, this paper proposes shape prior $E_S(S)$ based on regional information, as the punishment of regional prior information during Retinex component decomposition of the image. It can be seen that shape prior is the sum of local variation deviations in direction x and y direction:

$$E_S(S) = \left\| \frac{\partial_x \cdot S}{(1/\Omega)\sum_\Omega \partial_x S + \varepsilon} \right\|_1 + \left\| \frac{\partial_y \cdot S}{(1/\Omega)\sum_\Omega \partial_y S + \varepsilon} \right\|_1 \tag{5}$$

The Retinex reflection component contains rich texture information of the object, based on the consistency of the texture. The distribution of reflection components is considered to be piecewise continuous, and the gradient distribution of reflection components can be fitted by Laplace distribution. In real images, due to the influence of noise, and the regional noise distribution is not consistent in the light source, low brightness and dark areas, the distribution prior of reflection component is used to constrain the piecewise continuity as the estimation and compensation of regional noise in this paper:

$$E_t(R) = \|\partial_x \cdot R\|_1 + \|\partial_y \cdot R\|_1 \tag{6}$$

According to the above formula, the prior information of reflection components is the L1 norm superposition of the gradient of reflection components in the X and Y directions, representing the continuous change of the gradient of reflection components in each region.

The irradiance component of the image has great mutation at the boundary point of the object and the light source. If the irradiance component distribution is limited to the piecewise smooth distribution, the estimation of the irradiance component of the white object and the illuminant will produce serious distortion. Illumination component prior can be estimated according to human visual effect, as follows,

$$1 - S = (1 - R) \cdot I + 1 \cdot (1 - I) \tag{7}$$

Where S is the original image, I is the image illumination component and R is the reflection components. The optimization estimation process can be analogous to the prior solution method of dark channel prior defogging optimization model [12] as follows,

$$H = J \cdot T + \alpha(1 - T) \tag{8}$$

Where H is the fog image, T is the fog estimator and α is the atmospheric transmittance. The defogging algorithm uses dark channel prior to predict the transmittance T. In this paper, the illuminance component I is solved by using a similar method to approximate the maximum value of RGB three channels in ω as much as possible, which is:

$$I = 1 - \min_\Omega \left(\min_{c \in \{r,g,b\}} (1 - S)^c \right) = \min_\Omega \left(\min_{c \in \{r,g,b\}} S^c \right) \tag{9}$$

Therefore, the prior $E_1(I)$ of the illuminance component is defined as follows. The value of the illuminance component in each region is constrained to approach the maximum number of channels to punish the brightness information of the illuminance component.

$$E_1(I) = \left\| I - \max_\Omega \left(\max_{c \in \{r,g,b\}} S^c \right) \right\|_2^2 \tag{10}$$

According to shape prior, illuminance prior and reflection prior information, global optimization functions are defined to estimate I and R, as shown in Eq. (10). α, β and λ are the weight super-parameters corresponding to the three priors. When the value is too large, the punishment of prior information is excessive, leading to the filtering of regions with low brightness and locally uneven parts. When the value is too small, the re term is not penalized enough.

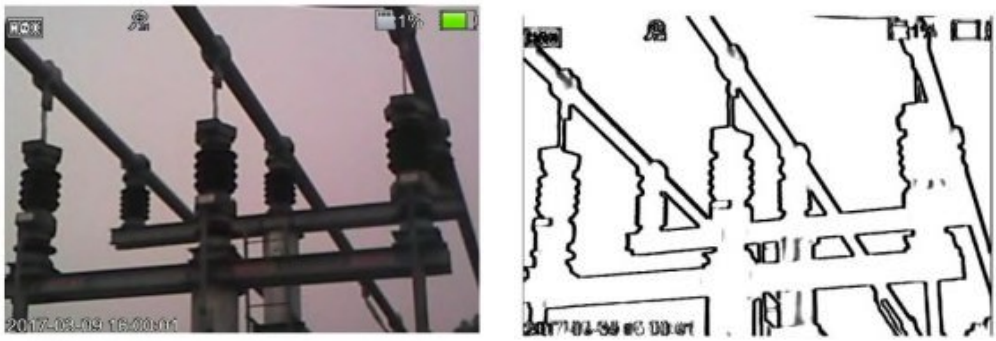

(a) Original image (b) Recognition of structure and edge

Fig. 1. Identifying edge areas using local variations

$$E(I,R) = \|I \cdot R - S\|_2^2 + \lambda E_1(I) + \alpha E_s(S) + \beta E_I(R) \quad (11)$$

Based on the hyperparameter values in reference [11], this paper selects appropriate hyperparameters α, β and λ , which are 0.01, 0.01 and 0.25, respectively, according to the experimental experience. Iterative re-weighted least square method [13] is adopted to modify the shape prior and reflection prior to L2 norm expression to solve the problem that non-smooth function is difficult to optimize. The block coordinate descent method [14] is used to solve the local minimum of the non-convex global optimization formula, and the estimated values of illumination component I and reflection component R after K iterations were obtained:

$$R_k = \arg\min_I (I_k \cdot R - S)^2 + \beta \left(w_x \cdot \|\partial_x R\|_2^2 + w_y \cdot \|\partial_y R\|_2^2 \right) \quad (12)$$

Where the size of nonlinear weights $u_{x/y}$ and $w_{x/y}$ as follows.

$$u_{x/y} = \left(\left| \frac{1}{\Omega} \sum_{\Omega} \partial_{x/y} S \right| \cdot |\partial_x S| + \varepsilon \right)^{-1} \quad (13)$$

$$w_{x/y} = \left(\partial_{x/y} R + \varepsilon \right)^{-1} \quad (14)$$

Fig. 2 show the original infrared heat map, the illumination component estimators and reflection component estimators respectively solved by the algorithm in this paper. It can be seen that the illuminance component presents the brightness information of the image and represents the gray difference between adjacent pixels, with high estimation accuracy. The reflection component represents the structural characteristics of the object, as well as the texture details of the object.

2.3. Gamma transform

Infrared heat map has the characteristic of small dynamic temperature range, resulting in a small gray difference between the target device and the background interference, and difficult to capture details. When the contrast of infrared heat map is improved, on the one hand, the image texture and illumination are estimated and compensated by combining prior information to eliminate the influence of noise [15, 16]. On the other hand, gamma transformation is performed on the estimated illuminance component to control the natural transition of gray stretching [17], the formula is as follows.

$$I' = I^{1/\gamma} \quad (15)$$

Where I is the irradiance component estimated by Retinex, $1/\gamma$ is the transformation coefficient. In this paper, the γ value in the gamma transform is set as 2.2, so that the gray gradient from black to white will look natural and uniform.

3. Multi-scale structure reserved smoothing filter

In complex environment, power equipment has the characteristics of low gray contrast, different structure size, more background interference, and multiple devices mixed. In the segmentation, we propose a multi-scale structure reserved smoothing filtering method based on the comparison enhancement of the heat map by using Retinex improved model in the previous chapter, which uses the proportion adjustment of coarse and fine scale characteristic deviation parameter σ .

It can not only filter the grayscale image of power equipment, eliminate the grayscale anomaly in the equipment, but also adjust the size of the filter in each area while protecting the edge of the structure from dispersion.

In Gaussian filter G_σ , the standard deviation σ determines the filtering radius [18]. Inspired by this, in order to

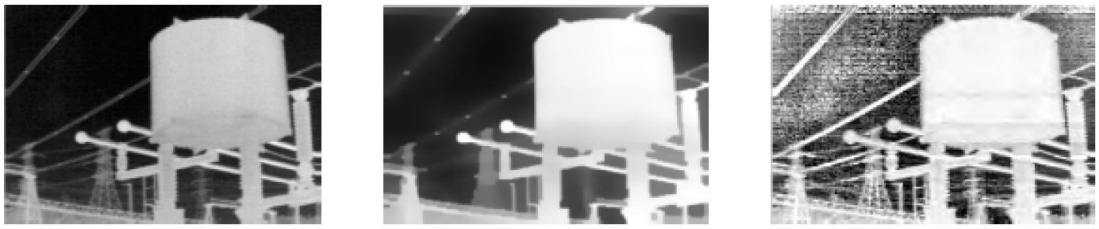

(a) Infrared heat map (b) Illuminance estimator (c) Reflection estimator

Fig. 2. The results of component estimation with proposed method.

be applicable to devices of different scales and avoid the filtering of some small structural edges, the algorithm in this paper introduces a new Gaussian kernel standard deviation σ_2 , and defines the local regular term of smoothing filtering as:

$$\widetilde{R} = \left| \frac{G_{\sigma_1} \cdot \partial S}{G_{\sigma_2} \cdot \partial S} \right| \tag{16}$$

Where G_{σ_1} and G_{σ_2} are Gaussian convolution kernels used for controlling different filter sizes, which are defined as follows.b

$$G_{\sigma_{1/2}}(x,y) = \exp\left(-\frac{1}{2\sigma_{1/2}}\left((x-x_0)^2+(y-y_0)^2\right)\right) \tag{17}$$

Standard deviation σ is the parameter that controls the filter size, and limiting condition is $\sigma_1 < \sigma_2$. (x_0, y_0) is the center of the convolution kernel. Therefore, the solution of $|G_{\sigma_1} \cdot \partial S|$ in the local regular term is the characterization of fine scale features, which contains all the gradient information in the image. Moreover, $|G_{\sigma_2} \cdot \partial S|$ represents coarse scale features [19], which only contains gradient information for strong edge or structural features.

The local regular term $\widetilde{R}$ is transformed, and the nonlinear weight of $\widetilde{R}$ in the x direction and y direction is calculated as $w'_{x/y}$.

$$w'_{x/y} = G_{\sigma_{1/2}} \cdot \frac{1}{\left|\left(G_{\sigma_1} \cdot \partial_{x/y} S\right)\left(G_{\sigma_2} \cdot \partial_{x/y} S\right)\right|} \tag{18}$$

By smoothing the texture edges of different sizes of input image S and adding regular term constraints, the image representation after k iterations can be obtained as follows.

$$S^k = \arg\min_S \|S-I\|_2^2 + \lambda'\left(w_x\left\|\partial_x S^{k-1}\right\|_2^2 + w_y\left\|\partial_y S^{k-1}\right\|_2^2\right) \tag{19}$$

Where λ' is a hyperparameter of the weight of the regular term. The first term of the optimization formula is used to constrain the L2 norm [20] of input and export images, that is minimum Euclidean distance, which makes the generated chart and export chart basically the same. By controlling the proportion of the two parameters σ_1 and σ_2 in the Gaussian kernel, the filter size of the edge of small texture and small structure can be controlled without deformation of the strong edge, as shown in Fig. 3. The smaller σ_1/σ_2 denotes the larger filter radius of the image texture, and the larger the grayscale smoothing range, which is suitable for devices with obvious edges and large component sizes such as reactors (as shown in Fig. 5 and Example 2). The larger σ_1/σ_2 is, the smaller the filtering radius is, which is suitable for equipment with small components such as grounding switch (as shown in Fig. 3). At this point, if the filtering radius is too large, edge dispersion will occur on small components, as shown in Fig. 3(c).

After the multi-scale structure reserved filtering, the gray difference between foreground and background of the infrared heat map is obvious, and the gray anomaly points in each region of the image can be eliminated. Otsu algorithm is used to cut the gray threshold. The gray histogram is normalized and the mean value and variance are calculated.

The maximum constraint of the variance between foreground and background is used to determine the optimal threshold of the image, and then the binary image is obtained. Multiplied by the improved Retinex enhanced image above, the gray-enhanced segmentation map of the target device can be generated. Compared with the original image, the segmentation image removes the background interference, improves the gray scale range, and can directly observe the temperature anomalies after the conversion to color map, providing convenience for intelligent barrier removal.

4. Phase stretch transformation (pst)

Phase stretching transform (PST) simulates the propagation mode of electromagnetic wave in diffraction medium with twisted dispersion, and distinguishes pixels with different

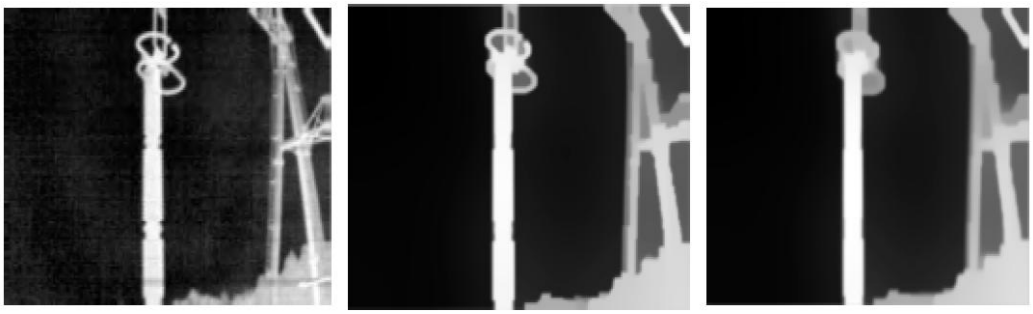

a)Enhanced image (b) $\sigma = 1, \sigma = 2$ (c) $\sigma = 1, \sigma = 3$

Fig. 3. Influence of deviation parameters σ on filter size

characteristics in the image. The phase transform in the frequency domain is helpful to detect the edge of the image and the position where the gray value of the pixel changes quickly. The edge information of the image contains higher frequency features. PST obtains the edge information of the image by emphasizing the higher frequency features, so as to enhance the edge information of the image.

$$A[n,m] = \angle < IFFT_2 \left\{ \widetilde{K}[p,q] \times FFT_2\{B[n,m]\} \right\} > \quad (20)$$

Where m and n are two-dimensional time domain variables. B $[n,m]$ is the input image; A$[n,m]$ is the output image. $\angle < \cdot >$ is the Angle operator. $FFT_2\{\}$ and $IFFT_2\{\}$ are Fourier transform and inverse Fourier transform respectively. p and q are two-dimensional frequency domain variables. $\widetilde{K}[p,q]$ is a nonlinear frequency correlation description, as shown in Eq. (21).

$$\widetilde{K}[p,q] = e^{j \times \varphi[p,q]} \quad (21)$$

5. Experiments and analysis

5.1. Enhancement results

In this paper, the improved gamma nonlinear transformation and single-scale Retinex algorithm are selected to compare with the image enhancement model in this paper, as shown in Fig. 4. The left half column is the grayscale diagram of equipment temperature. The darker color denotes the lower temperature. The right half of the column is the corresponding color map, where the cool to warm color transformation shows the temperature going from low to high.

In the experiment, the three hyperparameters α, β and λ of shape prior, reflection component prior and illumination component prior were set as 0.01, 0.01 and 0.25, respectively. Since the optimization formula is non-convex, the total number of iterations is set as 50 in this paper. At this point, the difference between the illuminance component or reflection component and the last iteration is close to 0.001, which is considered to be close to convergence. At this point, the local minimum value can be obtained.

It can be seen from Fig. 4(a) that the temperature difference between each area of the original infrared heat map equipment component is low, and it is difficult to directly observe the gray scale. Gamma nonlinear transformation adopts grayscale stretching of the global pixel value of the infrared heat map, resulting in a large amount of pixel grayscale accumulation in the mode region, uneven grayscale distribution, difficult to see temperature anomalies intuitively, and poor enhancement effect, as shown in Fig. 4(b).

As shown in Fig. 4(c), the single-scale Retinex image enhancement algorithm can stretch similar gray values to improve the contrast effect. However, the algorithm is easy to introduce noise during image enhancement, such as noise points in the background of color map in Fig. 4(c).

In practical application, it may lead to the change of gray value on the equipment, resulting in the wrong estimation of temperature anomaly. Compared with the previous two algorithms, the gray scale transition of image processed by the model proposed in this paper is natural and similar gray value can be distinguished. At the same time, the problem of amplification of noise points in optimization process is avoided by constraining the terms of reflection component prior information. From the perspective of processing effect, figure 4(d) is obviously superior to the experimental results of other algorithms.

5.2. Segmentation results

In order to verify the effectiveness of the segmentation algorithm in this paper in the segmentation of infrared heat maps of power equipment in complex environments and in response to different sizes and observation environments, we used the improved segmentation algorithm based on

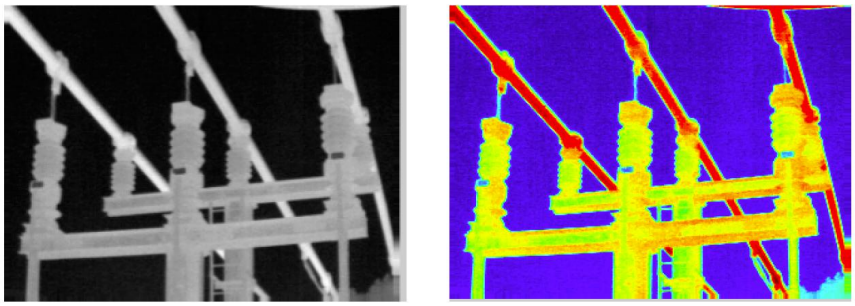

(a) Lightning arrester and its color map

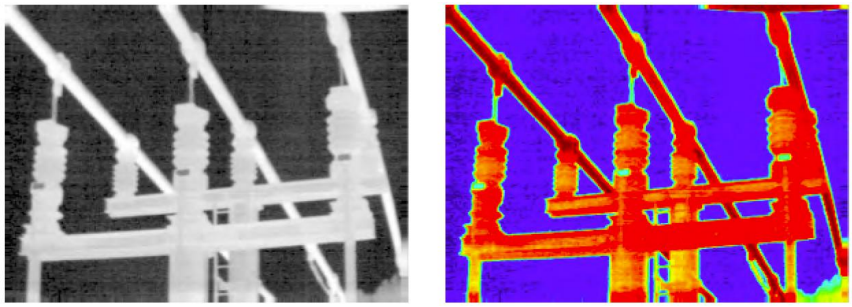

(b) Result of gamma nonlinear transformation enhancement

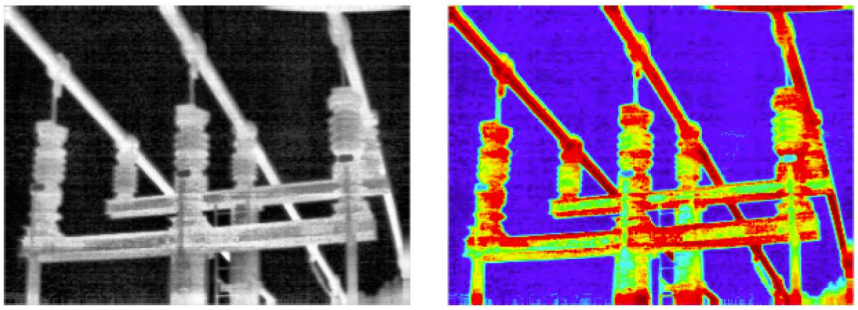

(c) Enhancement results with proposed method

Fig. 4. Comparison of enhancement results

Otsu in reference [21] as a comparison.

The standard deviation of the grounding switch set in the experiment is $\sigma_1 = 1, \quad \sigma_2 = 2$ (example 1 and example 3) respectively. Setting $\sigma_1 = 1, \quad \sigma_2 = 4$ in the reactor experiment (Example 2). The hyperparameter $\lambda^{'}$ of the weight of the regular term is set to 0.01, and the comparison results are shown in Fig. 5.

Fig. 6 shows the enlarged partial segmentation details of Fig. 5. From the comparison of detail edges [20, 21], it can be seen that the algorithm in this paper has good edge protection performance and can remove most background interference.

Fig. 5(a) $\sim$ (c) are original illustrations of power equipment taken in an outdoor environment, which are characterized by small gray difference between equipment components and diversified background interference. Fig. 5(a) $\sim$ (c) represent the state of three kinds of outdoor power equipment with background interference from small to large respectively.

Fig. 5(d) $\sim$ (f) is the result of image processing by using the segmentation algorithm. In the environment with less background interference, such as example 1 and 2, etc., the segmentation effect is certain, but the edge is still missing and the integrity of the equipment is damaged, as shown in Fig. 6(b) and Fig. 6(f).

In example 3, where there are many background interferences, there are a large number of background interferences whose grayscale is close to that of the target device, and there are still many interferences that cannot be removed after the algorithm is processed. Fig. 5(g)$\sim$(i) is the processing result of the algorithm in this paper on the infrared heat map.

It can be seen that the segmentation effect is good in complex environment, and a lot of background interference

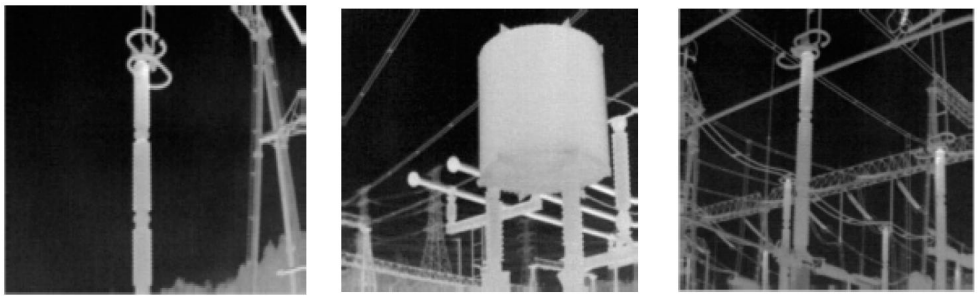

(a) Example 1 (b) Example 2 (c) Example 3

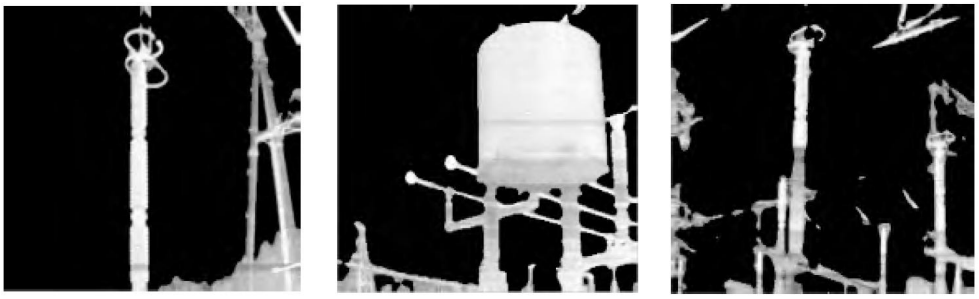

(d) Segmentation result of example 1 with [19]

(e) Segmentation result of example 2 with [19] (f) Segmentation result of example 3 with [19]

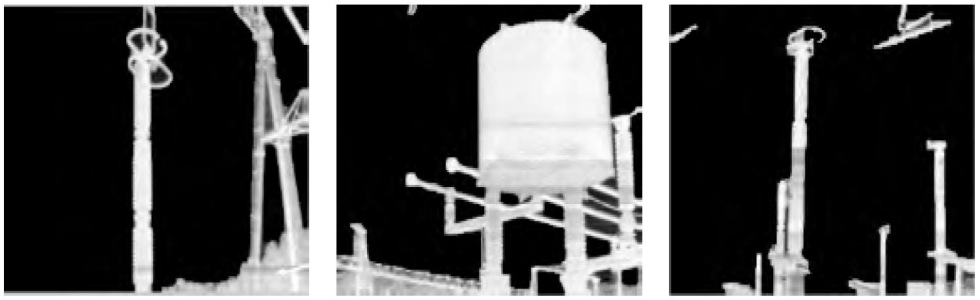

(g) Segmentation result of example 1 with proposed method (h) Segmentation result of example 2 with proposed method (i) Segmentation result of example 3 with proposed method

Fig. 5. Comparisons of model segmentation

Table 1. Time comparison/s

Data	Reference [19]	Reference [22]	Proposed
Example 1	2.9	1.7	0.6
Example 2	2.7	1.5	0.5
Example 3	2.1	1.8	0.7

is filtered out. In the environment with little background interference, the algorithm is also significantly better than other algorithms in processing the details of the back edge, and the edge structure of the segmentation graph is relatively complete, as shown in Fig. 6.

We also conduct the running time comparison as shown in table 1. We can see that the proposed method needs little time to segment one image.

6. Conclusions

Aiming at the characteristics of multi-interference, multi-noise and unequal size of power equipment in complex environment, a new enhancement and segmentation method is proposed in order to segment the heat map of equipment with complete structure and high contrast. The method compensates Retinex model with prior information on the basis of local variation bias, and obtains the regional estimators of illumination and noise. In the segmentation, multi-scale structure reserved flat slip filter is used to achieve the controllability of filter size, to ensure that the edge does not disperse, to achieve the integrity of segmentation, and in complex environment, most of the background interference can be filtered out. Experimental results show that the proposed algorithm can segment a complete and grayscale

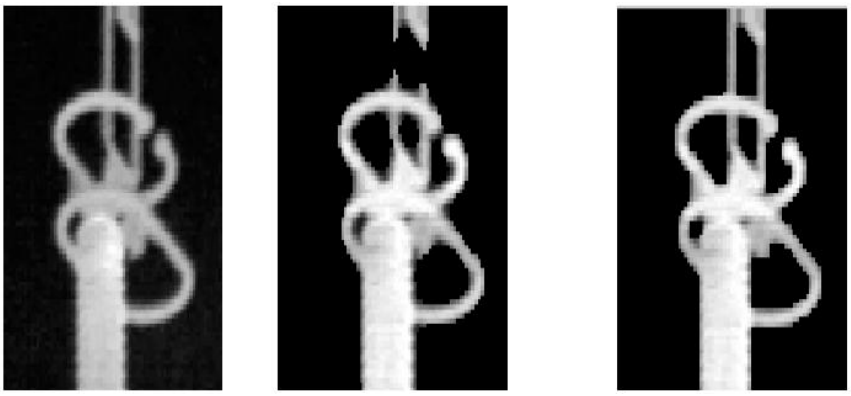

(a) Original image details (b) Image details of example 1 with [22] (c) Image details of example 1 with our method

(c) Original image details (f) Image details of example 2 with [22] (g) Image details of example 2 with our method

Fig. 6. Comparisons of model segmentation

enhanced infrared heat map of the target under the complex environment of power equipment operation, providing convenience for electricians to eliminate temperature fault points.

References

[1] H. Ren, X. Ye, J. Nie, J. Meng, W. Fan, Q. Qin, Y. Liang, and H. Liu, (2021) *"Retrieval of land surface temperature, emissivity, and atmospheric parameters from hyperspectral thermal infrared image using a feature-band linear-format hybrid algorithm"* **IEEE Transactions on Geoscience and Remote Sensing *60***: 1–15. DOI: 10.1109/TGRS.2020.3047381.

[2] Z. Zhang, H. Wang, T. Liu, Y. Wang, H. Zhang, F. Yuan, X. Yang, S. Xu, and Y. Meng, (2021) *"Accurate detection method of pig's temperature based on non-point source thermal infrared image"* **CAAI Transactions on Intelligence Technology *6***(3): 312–323. DOI: 10.1049/cit2.12017.

[3] D. Müller, A. Ehlen, and B. Valeske, (2021) *"Convolutional neural networks for semantic segmentation as a tool for multiclass face analysis in thermal infrared"* **Journal of nondestructive evaluation *40***(1): 1–10. DOI: 10.1007/s10921-020-00740-y.

[4] M. Younsi, M. Diaf, and P. Siarry, (2020) *"Automatic multiple moving humans detection and tracking in image sequences taken from a stationary thermal infrared camera"* **Expert Systems with Applications *146***: 113171. DOI: 10.1016/j.eswa.2019.113171.

[5] P. Zhuang and X. Ding, (2020) *"Underwater image enhancement using an edge-preserving filtering Retinex algorithm"* **Multimedia Tools and Applications *79***(25): 17257–17277. DOI: 10.1007/s11042-020-08739-3.

[6] H. Asmuni, R. M. Othman, R. Hassan, et al., (2013) *"An improved multiscale retinex algorithm for motion-blurred iris images to minimize the intra-individual variations"* **Pattern Recognition Letters *34***(9): 1071–1077. DOI: 10.1016/j.patrec.2013.02.017.

[7] S. Yin, Y. Zhang, and S. Karim, (2018) *"Large scale remote sensing image segmentation based on fuzzy region competition and Gaussian mixture model"* **IEEE Access *6***: 26069–26080. DOI: 10.1109/ACCESS.2018.2834960.

[8] Y. Li, G. Blois, F. Kazemifar, and K. Christensen. "A Particle-Based Image Segmentation Method for Phase Separation and Interface Detection in PIV Images of Multiphase Flow in Porous Media". In: 2021. DOI: 10.1088/1361-6501/abf0dc.

[9] H. Zou and F. Huang, (2016) *"Infrared image segmentation for electrical equipment based on fast-match algorithm"* **Infrared Technology** ***38***(1): 21–27.

[10] Q. Wang, J. Xue, and X. Ren, (2016) *"An Adaptive Segmentation Method of Substation Equipment Infrared Image"* **Infrared Technology** ***38***(09): 770–773.

[11] J. Frost, K. Keller, J. Lowe, T. Skeete, S. Walton, J. Castille, and N. Pal, (2013) *"A note on interval estimation of the standard deviation of a gamma population with applications to statistical quality control"* **Applied Mathematical Modelling** ***37***(4): 2580–2587. DOI: 10.1016/j.apm.2012.05.027.

[12] F. J. Franco, J. A. Clemente, M. Baylac, S. Rey, F. Villa, H. Mecha, J. A. Agapito, H. Puchner, G. Hubert, and R. Velazco, (2017) *"Statistical deviations from the theoretical only-SBU model to estimate MCU rates in SRAMs"* **IEEE Transactions on Nuclear Science** ***64***(8): 2152–2160. DOI: 10.1109/TNS.2017.2726938.

[13] E. J. Candes, M. B. Wakin, and S. P. Boyd, (2008) *"Enhancing sparsity by reweighted ℓ 1 minimization"* **Journal of Fourier analysis and applications** ***14***(5): 877–905.

[14] P. Tseng, (2001) *"Convergence of a block coordinate descent method for nondifferentiable minimization"* **Journal of optimization theory and applications** ***109***(3): 475–494. DOI: 10.1023/A:1017501703105.

[15] Q. Shi, S. Yin, K. Wang, L. Teng, and H. Li, (2021) *"Multichannel convolutional neural network-based fuzzy active contour model for medical image segmentation"* **Evolving Systems**: 1–15. DOI: 10.1007/s12530-021-09392-3.

[16] A. Jisi, S. Yin, et al., (2021) *"A new feature fusion network for student behavior recognition in education"* **Journal of Applied Science and Engineering** ***24***(2): 133–140. DOI: 10.6180/jase.202104_24(2).0002.

[17] H. Ahmad, S. K. Kim, J. H. Park, and S. Y. Jung, (2022) *"Development of two-phase flow regime map for thermally stimulated flows using deep learning and image segmentation technique"* **International Journal of Multiphase Flow** ***146***: 103869. DOI: 10.1016/j.ijmultiphaseflow.2021.103869.

[18] S. Gite, A. Mishra, and K. Kotecha, (2022) *"Enhanced lung image segmentation using deep learning"* **Neural Computing and Applications**: 1–15. DOI: 10.1007/s00521-021-06719-8.

[19] X. Fu, B. Fang, M. Zhou, and S. Kwong, (2021) *"Active contour driven by adaptively weighted signed pressure force combined with Legendre polynomial for image segmentation"* **Information Sciences** ***564***: 327–342. DOI: 10.1016/j.ins.2021.02.019.

[20] Z. B. W. Yiquan and J. Shouxin, (2010) *"Infrared image enhancement method based on stationary wavelet transformation and Retinex"* **Acta Optica Sinica**: DOI: 10.3788/AOS20103010.2788.

[21] J. Sun, (2021) *"Application of Image Segmentation Algorithm Based on Partial Differential Equation in Legal Case Text Classification"* **Advances in Mathematical Physics** ***2021***: DOI: 10.1155/2021/4062200.

[22] Y. Feng, H. Zhao, X. Li, X. Zhang, and H. Li, (2017) *"A multi-scale 3D Otsu thresholding algorithm for medical image segmentation"* **Digital Signal Processing** ***60***: 186–199. DOI: 10.13229/j.cnki.jdxbgxb201701037.